Self-consistent coupling of cavitation bubbles in aqueous systems

Moshe Strauss,[a] Yitzhak Kaufman, and Micha Sapir
Nuclear Research Center, Negev, P.O. Box 9001, Beer Sheva, Israel

Peter A. Amendt and Richard A. London
Lawrence Livermore National Laboratory, Livermore, California 94550

Michael E. Glinsky
BHP Petroleum, Houston, Texas 77056

(Received 28 August 2001; accepted for publication 9 January 2002)

The dynamics of an ensemble of cavitation voids initiated by laser-produced stress waves in aqueous systems is considered. Aqueous systems have large similarity to soft tissues. Laser-initiated stress waves are reflected from tissue boundaries, thereby inducing a tensile stress that is responsible for tissue damage. The early stage of damage is represented by an ensemble of voids or bubbles that nucleate and grow around impurities under stress wave tension. For impurity densities larger than 10^5 cm^{-3} the bubbles growth reduces the tensile wave component and causes the pressure to oscillate between tension and compression. For impurity densities below 10^8 cm^{-3} the bubbles grow on a long time scale ($\sim$10 μs) relative to the wave interaction time ($\sim$100 ns). For bubble densities above 10^8 cm^{-3} the bubble lifetime is greatly shortened because of the reduced tensile component. On a long time scale the growing bubbles cause a significant reduction in the liquid average compression pressure below the ambient atmospheric pressure. This effect increases the bubble lifetime by almost a factor of 2 relative to the low impurity density case when the bubbles are growing independently, in agreement with experiment [Paltauf and Schmidt-Kloiber, Appl. Phys. A: Mater. Sci. Process. **62**, 303 (1996)]. As the collapse stage starts, small bubbles collapse first and the compression pressure screening becomes less effective, thereby accelerating the collapse of the larger bubbles and reducing the spread of the bubble lifetimes. [DOI: 10.1063/1.1456247]

I. INTRODUCTION

In many medical applications laser-initiated stress waves induce tensile waves, that are responsible for tissue damage.[1–2] Such phenomena are naturally related to studies of cavitation and vapor bubble dynamics in aqueous systems.[2,3] These studies have a long history in a variety of applications in liquid systems in relation to bubble expansion and collapse far from boundaries and next to free, rigid, and elastic boundaries.[3] Tensile stresses can be generated from laser deposition of energy on free aqueous systems boundaries and from diffraction of stress waves while propagating inside these systems.[1–3] The damage starts with an ensemble of nucleating microcavities or voids around existing impurities induced by tensile stresses.[4,5]

In this article we study the dynamics of an ensemble of cavitation voids or bubbles initiated by a laser-induced stress wave in an aqueous system. Previous work ignored the interaction between the bubbles and the liquid.[1] In the present work the liquid responds to the bubbles growth by changing its pressure, which affects the bubble expansion. This feedback between the bubbles and the liquid defines the self-consistent picture represented in this article.

The growing bubbles can affect stress wave propagation on a 100 ns time scale. On a 1 μs time scale, the voids interact nonlinearly through liquid pressure fluctuations, thereby affecting their dynamics and lifetimes.[1] Thus a self-consistent model for the short and long time scale coupling of the liquid and voids evolution, is required.

It was shown in the experiments of Paltauf and Schmidt-Kloiber[1] that for moderate laser fluences, the lifetime of bubbles becomes longer than calculated by almost a factor of 2. They mentioned the possibility that the increase in impurity density for a given fluence makes it invalid to assume that the bubbles are growing independently in an infinitely extended liquid.

In this article we find that void growth on a 100 ns time scale reduces the stress wave tension and results in an oscillation between tension and compression. Voids growing on a microsecond time scale interact with each other through the alteration of the density and pressure of the surrounding liquid. This interaction causes the system to reach an average compression pressure below the ambient atmospheric pressure. Thus, the bubble lifetimes increase by almost a factor of 2 relative to the low impurity density case when the bubbles are growing independently, consistent with the experimental results discussed above. We further find that smaller bubbles collapse earlier and cause an increase in the average liquid pressure, which limits the lifetimes of larger bubbles.

The article is organized as follows: Section II presents the coupling between the hydrodynamics of the system and

[a]Author to whom correspondence should be addressed; electronic mail: mstrauss@netvision.net.il

the evolving of an ensemble of voids. Section III presents the computational results, and concluding remarks are given in Sec. IV.

II. COUPLING OF LIQUID HYDRODYNAMICS AND VOIDS EVOLUTION

A. Evolution of an ensemble of voids

We consider a bipolar stress wave generated on the free boundary of an aqueous system by a short pulse laser. The liquid system is described by a one-dimensional hydrodynamic code coupled to an ensemble of embedded impurities, which produce a distribution of voids under tension in the liquid.[4,5] The distribution of impurity sizes can be modeled as an exponential[4]

$$n(R)=\frac{n_0}{R_1}\exp(-R/R_1), \tag{1}$$

where $n\cdot dR$ is the number of impurities per unit volume with radius R in the range dR, n_0 is the impurity number density, and R_1 is the characteristic size. Typical values are $n_0\sim 10^5-10^8$ cm^{-3} and $R\sim 0.1-2$ μm. There are no limitations on the types of impurity distributions. The surface tension $2\gamma/R$ limits the nucleation threshold, where γ is the surface tension parameter. In water $\gamma=70$ erg/cm^2 and for tensions larger than 10 bar voids can nucleate around impurities with radius $R>0.15$ μm.

The hydrodynamic simulation solves for the ensemble of growing voids in every spatial zone at each time step. The voids grow as spherical bubbles around the impurities according to an extended Rayleigh model based on the Kirkwood–Bethe hypothesis.[6–9] The corresponding ordinary differential equation for the bubble radius R is[1,8,9]

$$R\dot{U}(1-M)+\frac{3}{2}U^2\left(1-\frac{M}{3}\right)$$

$$=\Delta H\cdot(1+M)+\frac{R}{C_s}\Delta\dot{H}\cdot(1-M), \tag{2}$$

where U is the bubble boundary velocity, $M=U/C_s$ is the Mach number, and C_s is the adiabatic sound speed. The enthalpy difference is $\Delta H\equiv H(R)-H_a=\int_{P_a}^{P(R)}(dp/\rho)$, where the enthalpy $H(R)$ and the pressure $P(R)$ are defined at the bubble boundary, and ρ is the liquid density. The enthalpy H_a and the ambient pressure P_a are taken as the local time-dependent liquid values obtained from the hydrodynamic simulation. The enthalpies can be written as $H(R)=[\varepsilon+(P/\rho)]_{r=R}$ and $H_a=[\varepsilon+(P/\rho)]_{r=r_a}$, where ε is the energy per unit mass. The pressure $P(R)$ on the bubble boundary depends on the pressure P_b inside the bubble, the surface tension γ, and the viscosity η,

$$P(R)=P_b(R,S_b)-\frac{2\gamma}{R}-4\eta\frac{U}{R},$$

where $\eta=10^{-2}$ erg s cm^{-3} for water. The first term on the right hand side of Eq. (2) depends on the difference between the pressure inside the bubble and the ambient pressure. For small density changes one obtains $\Delta H\approx[P(R)-P_a]/\rho$, and by inserting this approximation into Eq. (2) we obtain a more familiar though less accurate form of the extended Rayleigh equation.[7] The second term on the right hand side depends on the rate of change of the enthalpy and represents the acoustic emission by the bubble. Equation (2) can be applied for large levels of acoustic emission for Mach numbers on the order of unity.

The growing bubbles interact with each other when they are relatively small by modifying the liquid density and pressure surrounding them. When the void volumes become linked together, coalescence of the bubbles is obtained.[10] In a real tissue, the growing voids reduce the tissue strength and may coalesce to produce a complete fracture. In this work the bubbles are assumed to remain far from the coalescence stage which is a subject of future work.

B. Hydrodynamic model coupled to the void evolution

In the hydrodynamic model, the liquid system including the voids behaves as a porous material with an average density $\rho_{\rm av}$ that differs from the local liquid density ρ. The two densities are related by

$$\rho_{\rm av}=\rho\frac{(1-\theta_\nu)}{(1-\theta_{\nu 0})}, \tag{3}$$

where $\theta_\nu(t)$ is the local relative void volume, and $\theta_{\nu 0}(t=0)$ is the initial relative volume of the impurities. The hydrodynamic computations are done with $\rho_{\rm av}$, while the thermodynamic quantities such as pressure, temperature, energy density, and entropy are calculated using the equation of state (EOS) according to the local fluid density ρ. The increase in the void volume causes an increase in the liquid density ρ relative to the average density $\rho_{\rm av}$, which reduces the tension in the system. This couples the hydrodynamic motion to the void evolution.

The ensemble of impurities is represented by N initial radii $R_i(0)$ at time $t=0$. The radii $R_i(t)$ evolve according to the extended Rayleigh model as in Eq. (2) and depend on the local hydrodynamic pressure P_a. Other void radii in the ensemble are obtained by linear interpolation from the calculated $R_i(t)$. This procedure is used to calculate the relative void volume $\theta_\nu(t)$.

When the bubble grows under tension, the pressure inside the bubble is reduced almost to zero. In the collapse stage of the bubble its volume is limited by the compressibility of the impurity inside the bubble. Assuming that the collapse is not highly symmetric, we ignore the rebound of the bubble and take its collapse energy as fully dissipated in the liquid. Only new tensile stresses can generate a bubble re-expansion. The EOS that we use is based on the NBS Steam Tables.[11] The conditions inside the bubble are obtained by using the Maxwell constructed EOS.[11] Outside the bubble, where tensile waves can exist, the Van der Waals EOS is selected.[11] The expansion of the bubbles is adiabatic and the adiabats are generated for the inside and outside of the bubbles, based on the initial conditions after the heating of the system by the laser.

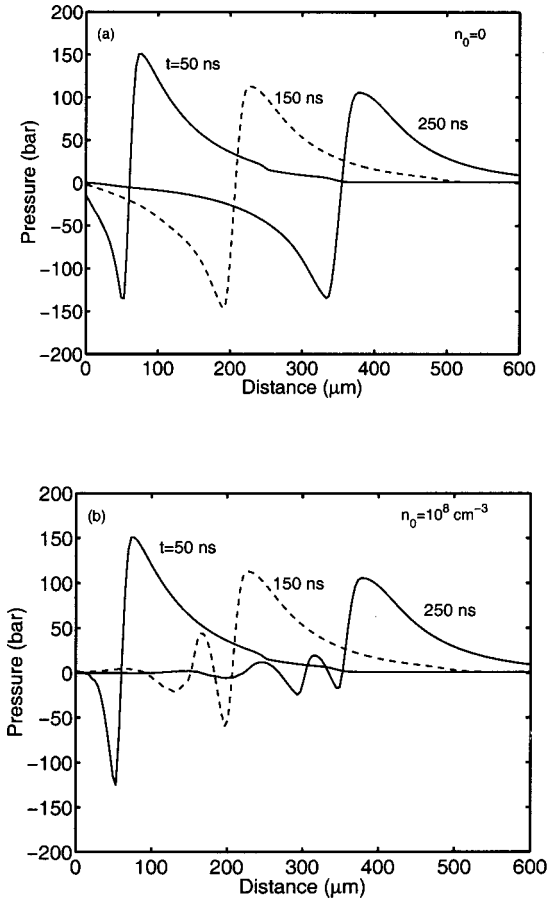

FIG. 1. Pressure vs distance for impurity density of: (a) $n_0 \approx 0$ and (b) $n_0 = 10^8$ cm^{-3} at times $t = 50$, 150, and 250 ns.

At the end of every time step and in every spatial hydrodynamic zone, the bubble radii and the relative void volume $\theta_\nu(t)$ are calculated based on the local hydrodynamic pressure. In the following time step $\theta_\nu(t)$ is used to transform ρ_{av} to the liquid density ρ according to Eq. (3). The density ρ and the temperature T are included in the iterations.

III. RESULTS AND DISCUSSION

In the hydrodynamic simulation we consider a short pulse laser beam incident on a free boundary of an aqueous liquid system. The laser energy is deposited exponentially with an absorption length l_a, heating the system from its initial temperature $T_0 = 20\,^\circ$C. The initial ambient pressure in the system is 1 bar. The laser heating generates a bipolar stress wave. The tensile component of the wave interacts with the ensemble of impurities and nucleates a distribution of growing voids. We consider an exponential distribution of impurities as in Eq. (1) with $R_1 = 0.5$ μm. We select five groups of impurities with initial radii $R_i = 0.3$, 0.5, 0.7, 1.0, and 1.5 μm. We find that the results are not sensitive to an increase in the number of groups.

For comparison with experimental results in Ref. 1 we select a laser fluence of 1.53 J/cm^2 and absorption length of 100 μm, which increases the liquid temperature at the free surface by 40 °C.

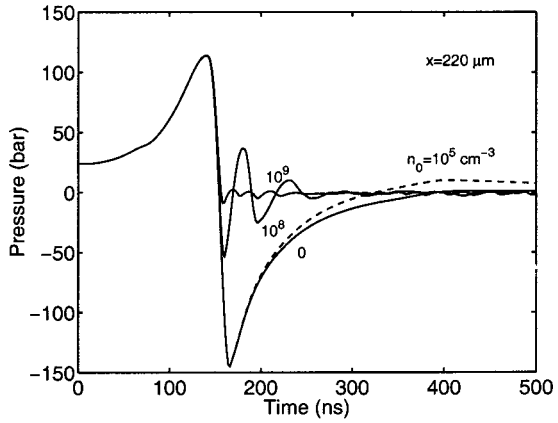

FIG. 2. Pressure vs time for impurity densities $n_0 = 0$, 10^5, 10^8, and 10^9 cm^{-3} at a distance of 220 μm from the free surface.

A. Short time scale dynamics

First consider the short time scale evolution on the order of $l_a/C_s \approx 100$ ns for impurity densities in the range $0 \leqslant n_0 \leqslant 10^9$ cm^{-3}. Figure 1(a) shows the stress wave pressure as a function of distance x from the free surface at times 50, 150, and 250 ns and for very low impurity concentration $n_0 \approx 0$. The bipolar wave is propagating almost unaltered through the system. Figure 1(b) considers the stress wave propagation for a moderate impurity density $n_0 = 10^8$ cm^{-3}. As the wave propagates inside the system the void growth imposes a reduction in the tensile component and causes the pressure to oscillate between tension and compression. The pressure oscillations are related to the density variation as the voids change their volume.

Figure 2 shows a time dependent comparison of the stress wave pressure for densities $n_0 = 0$, 10^5, 10^8, and 10^9 cm^{-3} at $x = 220$ μm. An increase in impurity density to $n_0 = 10^9$ cm^{-3} almost completely screens the tensile component on the time scale of stress wave propagation. The

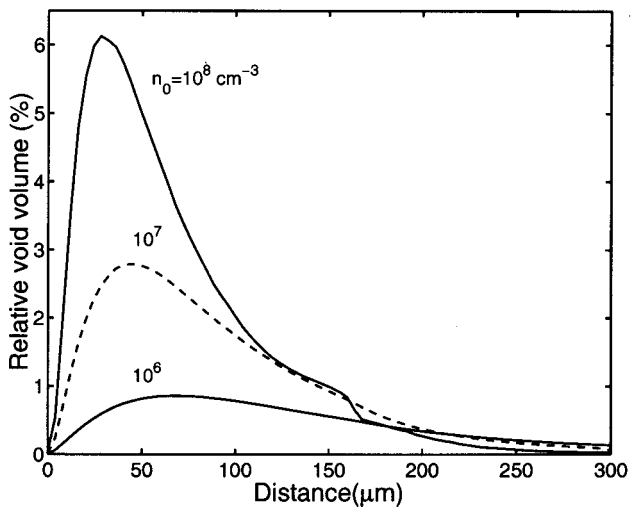

FIG. 3. The bubbles relative void volume (%) vs distance for impurity densities $n_0 = 10^6$, 10^7, and 10^8 cm^{-3} at time 500 ns.

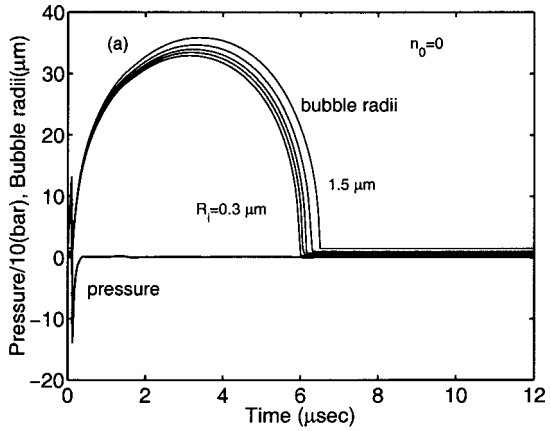

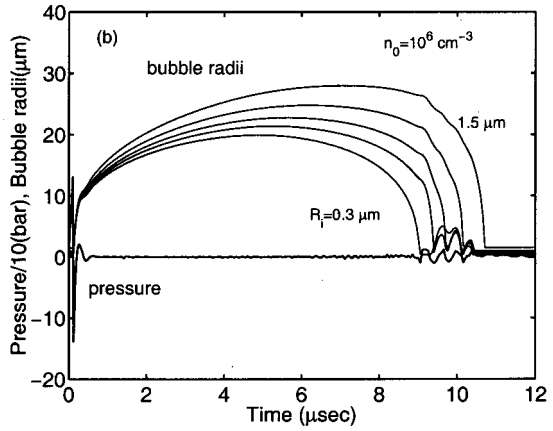

FIG. 4. Pressure/10 and bubble radii with initial values $R_i = 0.3$, 0.5, 0.7, 1.0, and 1.5 μm vs time at $x = 160$ μm for impurity densities of: (a) $n_0 = 0$ and (b) $n_0 = 10^6$ cm^{-3}.

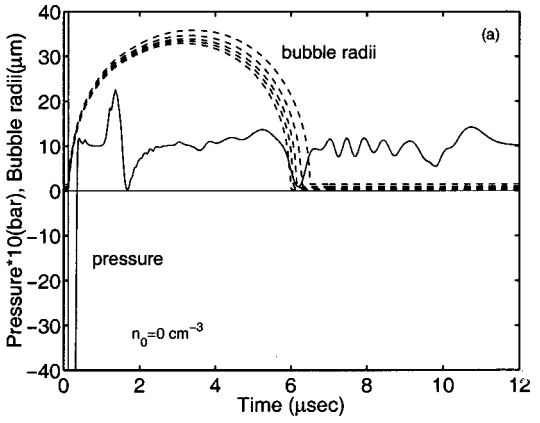

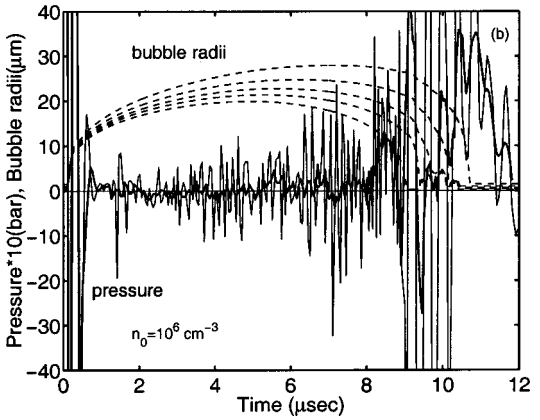

FIG. 5. Pressure$\times$10 and bubble radii as in Fig. 4 (dashed lines) vs time at $x = 160$ μm for impurity densities of: (a) $n_0 = 0$ and (b) $n_0 = 10^6$ cm^{-3}. In (b) we include the short time scale average pressure (bold line).

screening of the stress wave for densities below 10^5 cm^{-3} is small.

Figure 3 shows the relative bubble volume θ_ν as a function of distance from the free boundary for impurity densities $n_0 = 10^6$, 10^7, and 10^8 cm^{-3} at time 500 ns. As the impurity density increases, the maximum void volume increases, but less than linearly due to bubble interactions. As the impurity density increases there is a rapid decrease of the void volume versus distance from its maximum value. This is caused by the increased screening of the tensile component of the propagating stress wave by the bubbles [See Fig. 1(b)].

B. Long time scale dynamics

In the following we consider a long time-scale evolution on the order of the bubble lifetimes (microseconds). Figures 4(a) and 4(b) show the bipolar wave pressure (with a factor of 10 reduced scale) and a selection of bubble radii with initial values of $R_i(0) = 0.3$, 0.5, 0.7, 1.0, and 1.5 μm as a function of time for low impurity concentrations, $n_0 \approx 0$ and $n_0 = 10^6$ cm^{-3}, at a distance $x = 160$ μm from the boundary. In Fig. 4(a) the bubbles grow without interaction and collapse on a timescale of about 6 μs. The collapse is due to the 1 bar ambient compression pressure in the aqueous system. The collapse times are similar for the various radii and are independent of the propagation distance x. Bubbles with different initial radii grow similarly because they expand to radii much larger than their initial values. Figure 4(b) shows the mutual influence of the stress wave and bubble growth for an impurity density $n_0 = 10^6$ cm^{-3} and an exponential distribution of impurities. Note that the bubble lifetime increases to 10 μs in Fig. 4(b) which is almost a factor of 2 longer than in the noninteracting case [Fig. 4(a)]. This result is consistent with the experimental results reported in Ref. 1.

In Figs. 5(a) and 5(b) we increase the pressure scales in Figs. 4(a) and 4(b) by a factor of 100 for clarity. In Fig. 5(b) we also include a short time scale average pressure (bold line). For the noninteracting case in Fig. 5(a) the long time scale average pressure is close to 1 bar. In Fig. 5(b) the growing bubbles interact with the liquid causing pressure oscillations between tension and compression. These fluctuations are due to the nonequilibrium nature of the bubble growth. We see that the bubble interaction causes the system to reach a short time average compression pressure much below 1 bar, thus increasing the bubble lifetimes. In Fig. 4(b) the bubbles with initially smaller radii collapse earlier and there is a larger spread in bubble lifetimes compared to Fig.

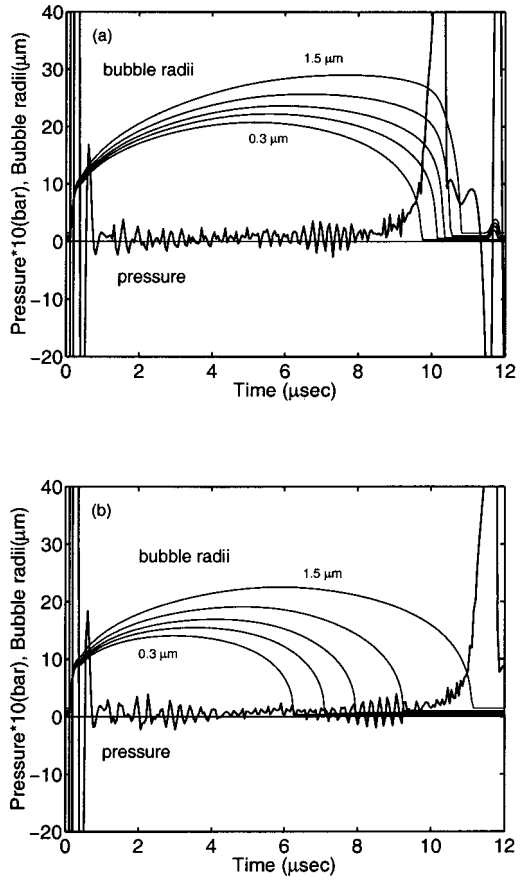

FIG. 6. Pressure×10 and bubble radii with initial values $R_i=0.3$, 0.5, 0.7, 1.0, and 1.5 μm vs time at $x=160\,\mu$m for impurity density of $n_0=10^6$ cm^{-3}. Almost all the impurities are initially equally distributed in the range: (a) 0.3–0.35 μm and (b) 1.45–1.5 μm.

4(a). In Fig. 5(b) when smaller bubbles start to collapse the reduction in the average compression pressure from bubble interactions becomes notably smaller after 8 μs. This pressure reduction limits any further increase in the lifetimes of larger bubbles and reduces the spread in the bubble lifetimes.

To study the mechanism that increases the bubble lifetimes we consider two more types of simplified impurity distributions in the range 0–1.5 μm. In Figs. 6(a) and 6(b)

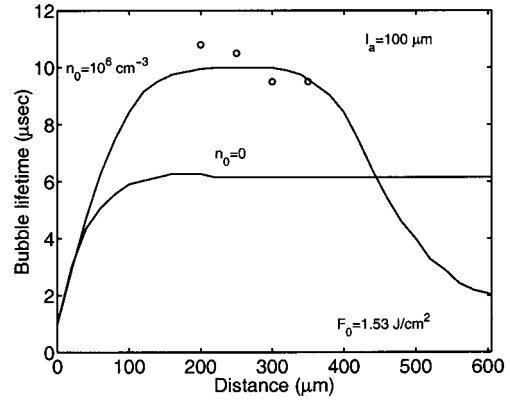

FIG. 7. Bubbles lifetime vs distance for bubbles with initial radius $R_i=1.0\,\mu$m, $n_0=10^6$ cm^{-3}, and $n_0\approx 0$. The laser fluence is 1.53 J/cm^2 and the absorption length $l_a=100\,\mu$m. The dots are the experimental results from Ref. 1.

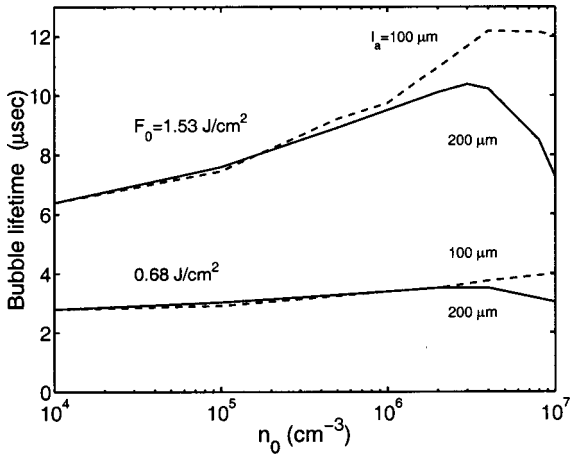

FIG. 8. Bubbles lifetime vs impurity density for bubbles with initial radius $R_i=1.0\,\mu$m, at a normalized distance $x/l_a=1.6$. The dashed line is for absorption length $l_a=100\,\mu$m and the solid line is for $l_a=200\,\mu$m.

we consider the majority of the impurities in uniform distributions with small radii in the range 0.3–0.35 μm and with larger radii in the range 1.45–1.5 μm, respectively. The pressure is represented on a larger scale by a factor of 10 to show its oscillatory nature and the fact that the average pressure is strongly reduced relative to the atmospheric pressure. This reduction is the main cause of the increase in the bubble lifetimes. In Fig. 6(a) bubbles with a smaller initial radii are in the majority and they strongly reduce the average compression pressure until a time of about 8 μs when the collapse stage starts, and lifetimes of about 10 μs are attained. Larger impurities that are in the minority attain similar bubble lifetimes, and the spread in the bubble distribution is small. As the collapse stage starts for the dominant smaller bubbles the average compression pressure is increased and the remaining larger bubbles collapse with only slightly larger lifetimes.

In Fig. 6(b) large bubbles are the majority and are more effective in screening the tensile component of the stress wave and the bubble initial growth is reduced. This causes the smaller bubbles to collapse earlier. But since they are relatively few in number, there is little effect on the collapse of the main bulk of larger bubbles. The larger bubbles reach higher lifetimes of more than 10 μs. In the expansion stage the average pressure is very low over a wide range of times. As the collapse stage starts the pressure is increased, causing larger bubbles to collapse in a short time relative to the expansion time. The spread in the bubble lifetimes is large.

In Fig. 7 we show the bubble lifetimes as a function of distance x from the free boundary for an absorption length $l_a=100\,\mu$m, a laser fluence of 1.53 J/cm^2 and densities $n_0\approx 0$ and 10^6 cm^{-3}. Figure 7 also includes the experimental results reported in Ref. 1. This fluence is consistent with a temperature rise at the free boundary of 40 °C. Comparing the lifetime results for bubbles with initial radius $R_i=1\,\mu$m, for $n_0\approx 0$, and $n_0=10^6$ cm^{-3}, there is an increase in lifetime from 6 to 10 μs for a wide range $100<x<350\,\mu$m. Good agreement is obtained for the bubble lifetimes between our computational results and experimental results of Ref. 1 for $n_0=10^6$ cm^{-3}. There is coupling be-

tween different locations in the liquid through the liquid pressure, clamping the bubble lifetimes to about 10 μs. It is clear that bubble interactions have a large influence on bubble lifetimes and should be calculated consistently with the bulk hydrodynamics. The lifetimes decrease for $x < 100$ μm where the tensile component is low and screened by the compression component. At larger distances, $x > 350$ μm, the lifetime is again reduced because the tensile component is attenuated by the voids growing at small x values.

Figure 8 considers the impurity density effect on the bubble lifetimes for bubbles with initial radius $R_i = 1$ μm, for absorption lengths $l_a = 100$ μm (dashed line), and 200 μm (solid line) at a dimensionless distance $x/l_a = 1.6$, for fluences 1.53 and 0.68 J/cm^2. For a fluence of 1.53 J/cm^2 there is an increase in bubble lifetimes with increasing impurity density, because of the strong reduction in the compression pressure relative to the atmospheric pressure. For this fluence the bubble lifetimes slowly increase up to densities of 5×10^6 cm^{-3}. At densities above 5×10^6 cm^{-3} pressure screening of the tensile stress is increased and the bubble lifetimes are reduced. This effect is stronger for $l_a = 200$ μm. For a smaller fluence of 0.68 J/cm^2, the bubble lifetimes are shorter and have a much weaker dependence on the impurity density. The results for 0.68 J/cm^2 are consistent with experimental results.[1]

IV. CONCLUSIONS

In conclusion we find that for aqueous systems with impurity densities 10^7-10^9 cm^{-3} there is a strong interaction between the stress wave and the ensemble of evolving voids on the short time scale of stress wave propagation ($\sim$100 ns). The interaction attenuates the stress wave tensile component and affects the bubble lifetimes. For impurity densities as low as 10^6 cm^{-3} the growing voids interact with each other on a longer time scale ($\sim$10 μs) through the change in the fluid pressure and strongly influence their lifetimes. Thus, bubble evolution should be treated self-consistently with the hydrodynamic pressure in the liquid even well before the onset of coalescence.[1] We find that various types of impurities with different initial radii nucleate voids that evolve on different time scales.

More experiments should be done with different impurity densities and different distributions to verify the interaction between stress wave propagation and bubble evolution. This effect should be extended to the coalescence stage in a liquid. The self-consistent effect of stress wave propagation and void evolution should be tested in real tissues for different physical effects such as viscosity, elasticity, and strength and failure mechanisms.

ACKNOWLEDGMENT

Part of this work was performed under the auspices of the U.S. Department of Energy by the University of California Lawrence Livermore National Laboratory under Contract No. W-7405-ENG-48.

[1] G. Paltauf and H. Schmidt-Kloiber, Appl. Phys. A: Mater. Sci. Process. **62**, 303 (1996).
[2] A. Vogel, S. Busch, K. Jungnickel, and R. Birngruber, Lasers Surg. Med. **15**, 32 (1994); G. Paltauf and H. Schmidt-Kloiber, Proc. SPIE **2391**, 403 (1995); T. G. van Leeuwen, E. D. Jansen, M. Motamedi, C. Borst, and A. J. Welch, in *Optical-Thermal Response of Laser Irradiated Tissue*, edited by A. J. Welch and M. J. C. Van Gemert (Plenum, New York, 1995), p. 709; A. Vogel, R. Engelhardt, U. Behnle, and U. Parlitz, Appl. Phys. B: Lasers Opt. **62**, 173 (1996); U. Sathyam, A. Shearin, and S. A. Prahl, Proc. SPIE **2671**, 28 (1996); M. Strauss, P. A. Amendt, R. A. London, D. J. Maitland, M. E. Glinsky, C. P. Lin, and M. W. Kelly, *ibid.* **2975**, 261 (1997); E. J. Chapyak, R. P. Godwin, S. A. Prahl, and H. Shangguan, *ibid.* **2970**, 28 (1997); R. P. Godwin, E. J. Chapyak, S. A. Prahl, and H. Shangguan, *ibid.* **3245**, 4 (1998).
[3] E. A. Brujan, K. Nahen, P. Schmidt, and A. Vogel, J. Fluid Mech. **433**, 251 (2001); A. Oraevsky and S. L. Jacques, J. Appl. Phys. **78**, 1281 (1995); M. Frenz, G. Paltauf, and H. Schmidt-Kloiber, Phys. Rev. Lett. **76**, 3546 (1996); P. Celliers, L. Da Silva, N. J. Heredia, B. M. Mammini, R. A. London, and M. Strauss, Proc. SPIE **2671**, 11 (1996); A. Prosperetti and J. W. Jacobs, J. Comput. Phys. **51**, 365 (1983); J. R. Blake and D. C. Gibson, J. Fluid Mech. **111**, 123 (1981); J. R. Blake, B. B. Taib, and G. Doherty, *ibid.* **170**, 479 (1986).
[4] D. R. Curran, L. Seaman, and D. A. Shockey, Phys. Rep. **147**, 253 (1987).
[5] M. E. Glinsky, D. S. Bailey, and R. A. London, Proc. SPIE **2975**, 374 (1997).
[6] Lord Rayleigh, Philos. Mag. **34**, 94 (1917); M. S. Plesset, J. Appl. Mech. **16**, 277 (1949); F. R. Gilmore, *California Institute of Technology*, Hydrodynamics Laboratory Report No. 26-4, 1950; L. Trilling, J. Appl. Mech. **23**, 14 (1952); R. Hickling and M. S. Plesset, Phys. Fluids **7**, 7 (1964); M. S. Plesset and A. Prosperetti, Annu. Rev. Fluid Mech. **9**, 145 (1977); W. Lauterborn, J. Acoust. Soc. Am. **59**, 283 (1976); A. Prosperetti, L. A. Crum, and K. W. Commander, *ibid.* **83**, 502 (1988); W. Lauterborn and U. Parlitz, *ibid.* **84**, 1975 (1988); C. E. Brennen, *Cavitation and Bubble Dynamics* (Oxford University Press, Oxford, 1995).
[7] R. T. Knapp, J. W. Daily, and F. G. Hammitt, *Cavitation* (McGraw–Hill, New York, 1966), p. 94.
[8] A. Vogel, S. Busch, and U. Parlitz, J. Acoust. Soc. Am. **100**, 148 (1996).
[9] M. E. Glinsky, D. S. Bailey, R. A. London, P. A. Amendt, A. M. Rubenchik, and M. Strauss, Phys. Fluids **13**, 20 (2001).
[10] D. Stauffer and A. Aharony, *Introduction to Percolation Theory*, (Taylor and Francis, London, 1992), M. Sahimi, *Application of Percolation Theory* (Taylor and Francis, London, 1994).
[11] L. Haar, J. S. Gallagher, and G. S. Kell, *NBS/NRC Steam Tables* (McGraw–Hill, New York, 1984).